

OPTIMIZING SOLAR RADIATION COEFFICIENT AS A SOLVE-FOR PARAMETER FOR THE ORBIT DETERMINATION PROCESS DURING THE LIBRATION-POINT ORBIT PHASE OF THE ARTEMIS MISSION

Jeffrey E. Marchese*, Daniel Cosgrove[†], Mark Woodard[‡], David Folta[§], Patrick Morinelli[¶], Brandon D. Owens^{||}, Sabine Frey^{**}, and Manfred Bester^{††}

The first two spacecraft to orbit Earth-Moon libration points—ARTEMIS P1 and P2—performed a total of 67 station-keeping maneuvers over a period of 10 months. With short durations between maneuvers and software restrictions that required data arcs be reset subsequent to each maneuver, it was critical to ensure that successive orbit determinations converged to an accurate solution in a timely manner. This paper details the in-flight techniques used to optimize solve-for parameters—such as the solar radiation coefficient, along with a constraint on its standard deviation—in the orbit solutions to ensure accuracy while still providing short convergence intervals. We present the collected data and we describe the application of our method for predicting orbit solution uncertainty in planning for the ARTEMIS Lunar orbit insertion operations.

INTRODUCTION

The ARTEMIS* mission was the first to maintain orbits in the Earth-Moon (EM) libration point regions—doing so about the co-linear libration points, EM L_1 and EM L_2 . The mission transferred the two outer-most probes of the five original THEMIS[†] spacecraft from their elliptical Earth orbits and, with lunar gravity assists, re-directed them to the libration points via transfer trajectories that exploit the Sun-Earth-Moon multi-body dynamical environment. The two identical ARTEMIS spacecraft, named P1 and P2, entered their libration-point orbits on August 25 and October 22, 2010, respectively. Once these orbits were achieved they were maintained for ~ 10 months, with the P1 spacecraft orbiting EM L_2 and P2 orbiting EM L_1 . During this libration-point orbit phase, P1 was transferred from L_2 to L_1 in early January, 2011. From these orbits, both spacecraft were inserted into elliptical lunar orbits on June 27 and July 17, 2011, respectively.¹

*Flight Dynamics Analyst, Space Sciences Laboratory, University of California, Berkeley, CA, USA.

[†]Navigation Lead, Space Sciences Laboratory, University of California, Berkeley, CA, USA.

[‡]Flight Dynamics Engineer, Navigation & Mission Design Branch, NASA GSFC, Greenbelt, MD, USA.

[§]Flight Dynamics Engineer, Navigation & Mission Design Branch, NASA GSFC, Greenbelt, MD, USA.

[¶]Orbit Analyst, Flight Dynamics Facility, Honeywell Technology Solutions Inc., Greenbelt, MD, USA.

^{||}Flight Dynamics Analyst, Space Sciences Laboratory, University of California, Berkeley, CA, USA.

**Mission Design Lead, Space Sciences Laboratory, University of California, Berkeley, CA, USA.

^{††}Director of Operations, Space Sciences Laboratory, University of California, Berkeley, CA, USA.

* ARTEMIS: Acceleration Reconnection and Turbulence and Electrodynamics of the Moon's Interaction with the Sun.

[†]THEMIS: Time History of Events and Macroscale Interactions during Substorms.

A significant task for the operations team during the libration-point orbit phase of the ARTEMIS mission was to generate daily orbit solutions (ODs^{*}) from ground station-obtained range and Doppler tracking measurements. To this end, an OD process—built around Goddard Space Flight Center’s GTDS[†] program—was utilized to publish ODs for monitoring the position and velocity of the spacecraft. This process has a limitation in that it does not function properly with continuous data obtained across maneuvers (or other significant orbital disturbances).

The period of each libration-point orbit was roughly 14 days. Most of the station-keeping maneuvers (SKMs) were performed on the half-period and were phased to the crossing of the Earth-Moon vector. After each SKM, the data arc was restarted with the end of thrusting for that maneuver. In each of these episodes, as the gathered data volume increased, the accuracy of the resulting OD increased.

Prior to the beginning of the libration-point orbit phase, key questions regarding the time required to achieve suitable accuracy were:

- How much data (i.e., ground station contact time) would need to be gathered?
- What balance of geographically distributed station data would be optimal?
- What effect would allowing the solar radiation coefficient to “float” as a dynamic solve-for variable have?

This paper focuses primarily on the last question, but the answers to the other two are considered, as well. Presented below is an exploration of the above questions in several sections. The next section provides *Background* with regard to the OD process, including some specifics of the models used and decisions made regarding our investigations. The *Method* section then details the statistical quantities and the approach taken to quantify our results. These are presented in the *Results* section. The *Applications* section discusses using the information gathered to plan maneuvers, such as the Lunar orbit insertion (LOI) phase—subsequent to the libration-point orbit phase. The *Discussion & Further Work* section is provided to explore interesting aspects of our findings and present our ideas for more study. The text of the paper is concluded with a section of *Summary and Conclusions*. *Appendix A: Glossary* provides definitions for the acronyms used herein. Figures and tables are found in *Appendix B: Figures* and *Appendix C: Tables*, respectively.

BACKGROUND

The Orbit Determination Process

Orbit determination through GTDS uses a batch-weighted, least-squares (differential correction) method to estimate the spacecraft orbit from received tracking data. The differential corrector solves for position, velocity, and (optionally) solar radiation coefficient C_R at the solution epoch. The operations team typically targets the solution epoch near the end of the arc. This sacrifices some accuracy (and solver stability) in the overall solution in exchange for better resolution near the most recent observations. Note that due to the nature of the least-squares method, the tracking arcs needed to be reset subsequent to each maneuver.

^{*}OD: Orbit determination. Also, orbit solution.

[†]GTDS: Goddard Trajectory Determination System is a government off-the-shelf software (GOTS) package developed at NASA’s Goddard Space Flight Center (GSFC)

The quality of a given solution is determined through statistical measures such as the root-mean-square (RMS) of the data as it relates to the solution. Beyond the solution RMS, the primary set of factors for judging OD quality are the 3- σ * values for either the orbital elements, or the position and velocity vector components. The former are useful for elliptical orbits, while the latter are required for orbits not defined by elliptical trajectories. We will refer to the full set or some specific subset of these 3- σ values as the *uncertainty* in the solution—since they refer to how well the solution is described by the accumulated data. (While not important for purposes of this paper, it should also be noted that OD quality is further judged on the basis of comparison to the previous orbit and by the aberrations of timings of known impending events.)

GTDS Solar radiation model

The GTDS solar radiation model includes shadowing and variations with the distance from the Sun. The force due to solar radiation pressure on a vehicle’s surface is dependent on the effective area A of the surface normal to the incident radiation, the surface reflectivity η , and the luminosity L_S of the Sun, the square of the distance R_S from the Sun, and the speed of light c . From these relationships, a proportionality constant, the coefficient of solar reflectivity C_R can be defined in terms of the resultant radial solar radiation pressure force:

$$F_R = C_R \frac{L_S A}{4\pi c R_S^2}, \quad (1)$$

with $C_R \equiv 1 + \eta$. For example, the coefficient of solar reflectivity for aluminium is $C_R = 1.95$.

Allowing the GTDS differential corrector to solve for C_R obviously has specific ramifications on the solutions generated. Not having to specify C_R (i.e., allowing it to be solved-for as a degree of freedom) is convenient in that one avoids introducing error in the knowledge of this quantity. Variations in solar activity and errors in knowledge of the spacecraft’s presented cross-sectional area all contribute to this uncertainty. But in allowing this value to be calculated, the differential corrector has an additional degree of freedom in which to aggregate error due to unmodeled forces. This places significance on giving the differential corrector a suitable initial, *a priori* value.²

As part of the OD profiling effort featured in this paper, we sought to apply considered analysis techniques to determine the optimal a priori value for C_R (C_R^0) during the libration-point orbit phase of the ARTEMIS mission. A second parameter—the initial standard deviation (σ^0) within which C_R is allowed to vary from the a priori value (in a *non-strict*, but meaningful sense)—is also provided by GTDS and was studied, as well.

It should be noted that while GTDS does allow for solution of C_R in an unconstrained fashion, constraining C_R ensures that the error for short tracking arc regimes is contained in the solution vector itself. Otherwise, the solution will obtain nonsensical values for the solved-for C_R . This is further examined in the Results section.

METHOD

In discussing convergence, we focus on two basic types: *solver convergence* and *planning convergence*. We define solver convergence in terms of the computational effort required to achieve a solution within a specified tolerance in a given number of iterations. Planning convergence is defined as the process of achieving reduced variance in dynamic fluctuations between successive ODs

*3- σ : The third standard deviation of a quantity outside of its mean.

which minimizes to an acceptable limit for maneuver planning purposes. For simplicity, we will refer to the latter as just *convergence*. A key metric in determining this latter type of convergence is the root sum square (RSS) of the 3- σ uncertainty in the in-plane velocity components V_x and V_y , represented by V_ϵ and otherwise denoted as *OD uncertainty*.

Figure B-1 plots OD uncertainties for P1 and P2 for solution epochs across the libration-point orbit phase. The red line in each panel depicts the average rate of convergence, a key metric in determining the suitability of OD solutions for use in maneuver planning and for profiling OD uncertainties for C_R^0 and σ^0 .

Prior to entering libration-point orbit, the [mission-proven] expertise of several key team members considered the goal for pre-maneuver OD uncertainty to be $\sim 10^{-2}$ cm/s.² Figure B-1 indicates that this level of accuracy was reachable with a reasonable amount of tracking data (roughly 5 days worth). Also note that the rate of decrease in OD uncertainty "tails off" with the collection of more data. Thus in determining the optimal values for C_R^0 and σ^0 , we established a method for maximizing the absolute value of the rate of convergence, while keeping solver convergence times within an hour or so.

Figure B-2 indicates that the form for the rate of convergence,

$$M(T) = \frac{\log_{10}\left(\frac{V_\epsilon}{V_\epsilon^0}\right)}{(T - T^0)}, \quad (2)$$

is suitable for our purposes. Here, V_ϵ^0 is the initial OD uncertainty at the initial number of tracking hours T^0 (subsequent to the considered SKM), and T is the number of tracking hours to date.

Figure B-3 plots C_R for P1 and P2 for solution epochs across the libration-point orbit phase. It is quite interesting that, as the OD uncertainty becomes acceptable (for maneuver planning) at around 30 hours of cumulative tracking time and the solutions converge, the C_R starts to diverge from the initial value—resulting in a noticeable increase in $\sigma(C_R)$. One possible explanation for this behavior is that as the data arc becomes extended across the orbit, the probability of unmodeled forces perturbing the orbit increases. This will be explored further in the Discussion & Future Work section. For our purposes though, the key illustration from Figure B-3 is that C_R stays relatively constant until the solutions converge. This constancy is useful for analytically varying the value for C_R^0 and σ^0 to determine the effect on convergence across the SKM data set.

To compare each OD sequence through ranges of C_R^0 and σ^0 we devised the following algorithm:

Establish a benchmark for each SKM sequence by examining the value of V_ϵ achieved after 25-30 hours of accumulated tracking data (the amount gathered during roughly one-third of the period, or 4-5 calendar days). This we call the *converged OD uncertainty* and we denote V_ϵ^C .

There were two complications to our strategy. First, the independent variable is discrete*. So in determining an average value for the entire sequence, we needed to ensure that the data associated with consistent tracking hours was used for each SKM, as C_R^0 and σ^0 were varied.

*Ground station data accumulation rates were not the same for every SKM sequence, as every period between SKMs had a unique tracking schedule

Also, since the independent variable is bounded by a *range*, we needed to resolve the cases where there were multiple values in the range, and where there were no values in the range. These conflicts were resolved as follows:

- In the case of multiple values in the range, the range-bound value of V_ϵ^C closest to 30 hours was used.
- In the case of no values in the range, the value of V_ϵ^C closest to the lower range limit was used.

Averaging these across a sequence of SKMs gives $\langle V_\epsilon^C \rangle$.

Figures B-4 through B-7 present overviews of the calculated C_R , OD uncertainty, and accumulated tracking time for the P1 and P2 SKM sequences through DOY 2011/115. Tracking time for stations in the southern hemisphere is illustrated with filled red circles.

In the next section we present the results of this method.

RESULTS

Figure B-8 demonstrates both the effect of leaving C_R^0 unconstrained and also gives some indication of the sensitivity of the solved-for C_R to the value given C_R^0 . Interesting features of this figure include:

- During the accumulation of the first 20 hours of tracking data, unconstrained solutions generally did not converge as quickly. After roughly 30 hours of tracking data, however, unconstrained solutions achieved similar levels of OD uncertainty to the constrained solutions.
- The value for C_R^0 is not highly critical with regard to convergence rate or the converged value for C_R .
- C_R for unconstrained solutions varies somewhat wildly until about 35-45 hours of tracking data.

While Figure B-8 makes it clear that there are no large effects to be found by fine tuning C_R^0 , we still wanted to explore the potential for optimization. Often we were hard pressed to gain tracking passes and we felt the need to make the process as efficient as possible. We present our fine tuning results in Tables C-1 through C-4.

Tables C-1 and C-3 portray the first pass of our method, which was to establish the minimum OD uncertainty at a constant $\sigma^0 = 1.0$. The optimal values were determined to be $C_R^0 = 1.14$ for P1 and $C_R^0 = 1.12$. The results of the second pass, where we tried to fine tune σ^0 , are shown in Tables C-2 and C-4. As one might expect, there is a limit to how tightly the solution can be constrained, and we see this with poor solver convergence with very small σ^0 . The data also confirm the slower convergence of the unconstrained solutions.

APPLICATIONS

The above results were used, along with Equation 2, to predict the OD uncertainty for anticipated operations based on the expected volume of tracking data. Figure B-9 is an example of how these predictions were employed.

This diagram is a snapshot of the planning document prepared one month prior to the LOI sequence and was helpful in ensuring that enough tracking data was secured for the maneuver preparation ODs.

Our aforementioned question regarding geographical data balance is [somewhat] addressed by Figure B-10. There seems to be an indication that the OD uncertainty usually falls below our threshold of $\sim 10^{-2}$ cm/s, regardless of hemispherical balance, as long as the total tracking time is more than 25 hours. While the trend shows that uncertainty is reduced with balanced tracking, there does not seem to be a strong correlation between convergence rate hemispherical balance.

DISCUSSION & FURTHER WORK

In this section we address some interesting features of the data we have presented and indicate areas where further, follow-up work may be conducted.

In Figure B-3 it is interesting that the standard deviation in the data increases quite significantly after convergence is reached (at about 30 hours of tracking data). This is most likely due to the fact that, at this level of tracking data, the OD uncertainty has reached a low enough level that errors from perturbations in the orbit are absorbed into the calculation for C_R . As tracking hours increase, small errors in the satellite's calculated path accumulate due to unmodeled forces such as solar effects from coronal mass ejections—which cause rapid, large-scale changes in Solar radiation pressure—and errors in the model for the Lunar potential. These types of errors are also most likely responsible for the rather large standard deviations in much of our data.

One may wonder why the z-component of velocity V_z was not included in our definition of OD uncertainty. In most of our OD solutions (even after convergence), the $3\text{-}\sigma$ value for V_z was usually an order of magnitude larger than V_x and V_y , so deviations in the in-plane velocities were masked by its inclusion. Also, it turned out that for most of the libration-point orbit ODs, proportionate reductions in V_z occurred as OD uncertainty decreased. So it was somewhat redundant information. A study of these types of errors for libration-point orbits is presented in Reference 3.

During the SKM sequence for P1 there was a transfer of the probe from EM L_1 to EM L_2 . Little work has been performed to date to examine differences in the data presented above. There were no apparent differences, but further analysis is needed for more definitive conclusions.

Further, an interesting feature of both Figures B-3 and B-8 is the [seemingly] bi-modal distribution seen in the calculated C_R for P1 at long accumulated tracking hours. When we first observed this feature, P1 was orbiting EM L_2 and we were curious to observe changes to this effect after the transfer to EM L_1 (since P2's orbit of EM L_1 had not shown this behavior.) We were mildly surprised to find the same bi-modal distribution for P1 throughout the libration-point orbit phase. Additional analysis is needed to explore the origin of this phenomena.

Also, we would be interested in eliciting from the data more information about OD performance with regard to the orbit phase angle distribution of the data. Note that our results are primarily based on data arcs which span less than one period worth of data. In elliptical orbits, GTDS works best with data arcs which are several periods long. One would expect that data arcs with more curvature should have more uncertainty than those with less, and that these differences would be larger for shorter data arcs.

SUMMARY AND CONCLUSION

In this paper we have presented the development of a technique that uses the solar radiation coefficient—in combination with a constraint on its standard deviation—as a solve-for parameter in the orbit solutions. During the mission we were able to use this method to provide metrics for establishing the quantity of tracking time needed for the planning of frequent station-keeping maneuvers. Additionally, we used these metrics to determine a suitable range for the balance of geographically distributed station data, allowing us to use our tracking resources efficiently without compromising quality.

A key finding here is a correlation between the standard deviation in calculated C_R and accumulated tracking hours. The discovered sharp increase of the standard deviation when the accumulated tracking time is of the order of the convergence period will be subject to further analysis in order to develop an orbit specific parameter for tracking schedules.

The ARTEMIS navigation and flight dynamics team used the above method to successfully guide P1 and P2 through the libration-orbit phase to Lunar orbit insertion—starting in August and October 2010 until June and July 2011, respectively. The data we collected and analyzed during this phase has also contributed to highly accurate ODs during the subsequent (and current) Lunar orbit phase of the mission, especially as we lower the average periselene of each probe to incur minimum altitudes below 20 km.

Hopefully, other missions intended for Earth-Moon libration-point orbits can benefit from the experience documented herein, and from other key learnings documented by the ARTEMIS team.

ACKNOWLEDGEMENTS

The authors would like to express their gratitude to Theodore (Ted) Sweetser and Stephen (Steve) Broschart, both of the Caltech Jet Propulsion Laboratory (JPL), for their contributions to this paper and to the ARTEMIS mission.

The THEMIS and ARTEMIS missions are operated by the University of California, Berkeley under NASA contract NAS5-02099.

APPENDIX A: GLOSSARY

3- σ : The third standard deviation of a quantity outside of its mean.

ARTEMIS: Acceleration Reconnection and Turbulence and Electrodynamics of the Moon's Interaction with the Sun.

DOY: Day-of-Year

GTDS: Goddard Trajectory Determination System: A government off-the-shelf software (GOTS) package developed at NASA's Goddard Space Flight Center (GSFC).

OD: Orbit Determination. Also, orbit solution.

THEMIS: Time History of Events and Macroscale Interactions during Substorms.

APPENDIX B: FIGURES

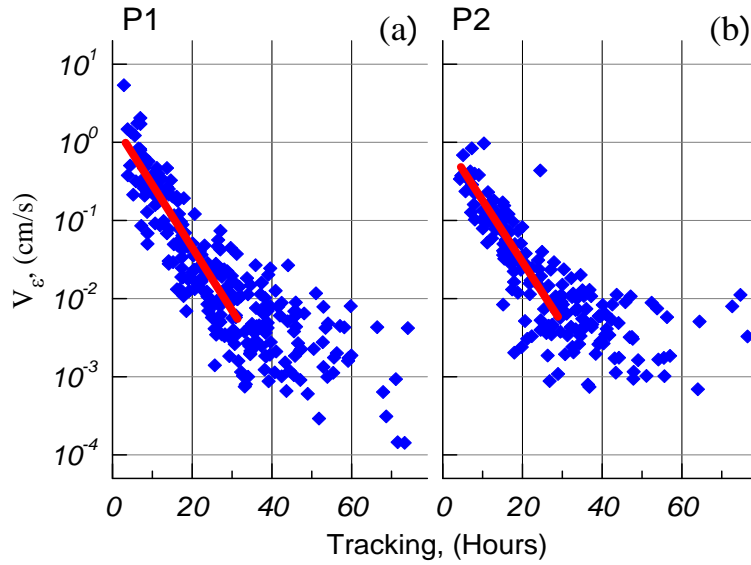


Figure B-1. OD uncertainty versus cumulative tracking hours, aggregated over the libration-point orbit phase through Day-of-Year (DOY) 2011/115 for P1 in panel (a), and P2 in panel (b). The red lines represent an approximate average descent rate in OD uncertainty. Parameters for P1 were: $C_R^0 = 1.14$, $\sigma^0 = 0.10$; and for P2 were: $C_R^0 = 1.12$, $\sigma^0 = 0.10$.

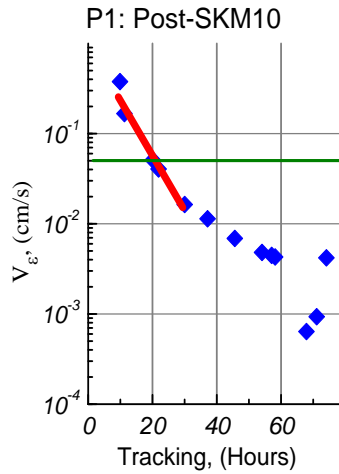


Figure B-2. OD uncertainty versus cumulative tracking hours for the P1 data arc, beginning after SKM10 on DOY 2010/321 and ending before SKM11 on DOY 2010/334. The red lines represent an approximate average descent rate in OD uncertainty. The green horizontal line represents the threshold of convergence. Parameters were: $C_R^0 = 1.14$, $\sigma^0 = 0.10$.

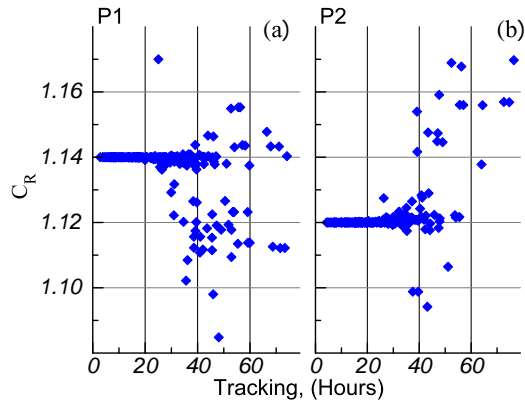


Figure B-3. C_R trending, aggregated over the libration-point orbit phase (through DOY 2011/115) for P1 in panel (a), and P2 in panel(b). Parameters for P1 were: $C_R^0 = 1.14$, $\sigma^0 = 0.10$; and for P2 were: $C_R^0 = 1.12$, $\sigma^0 = 0.10$.

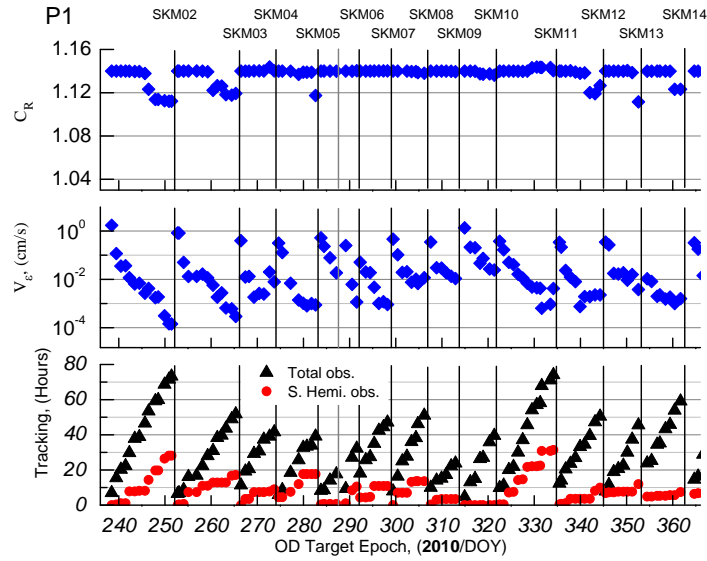


Figure B-4. Overview of P1 SKM sequence for 2010 with parameters: $C_R^0 = 1.14$, $\sigma^0 = 0.10$. Note there was a break in the tracking arc due to a dynamics event on P1 on DOY 2010/284.

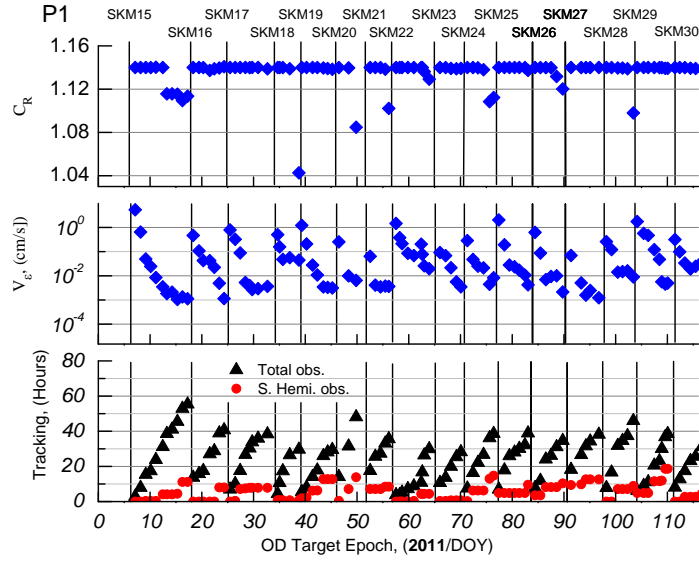


Figure B-5. Overview of P1 SKM sequence for 2011 (through DOY 115) with parameters: $C_R^0 = 1.14$, $\sigma^0 = 0.10$. Note that P1 transferred from EM L_2 to EM L_1 on DOY 2011/006.

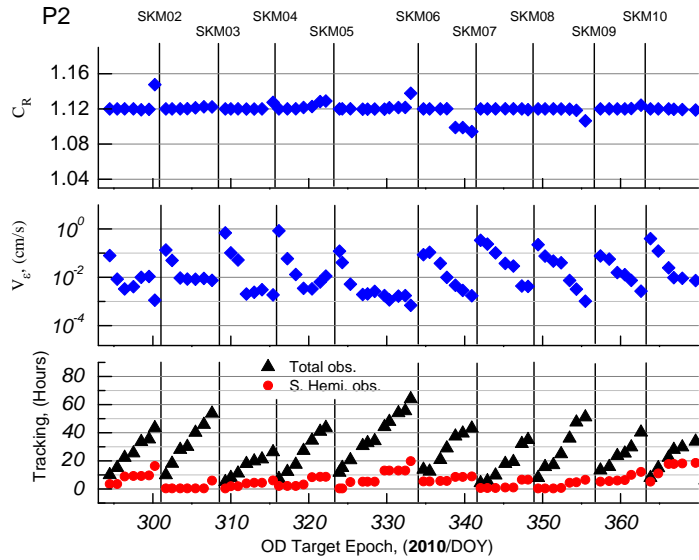


Figure B-6. Overview of P2 SKM sequence for 2010 with parameters: $C_R^0 = 1.12$, $\sigma^0 = 0.10$.

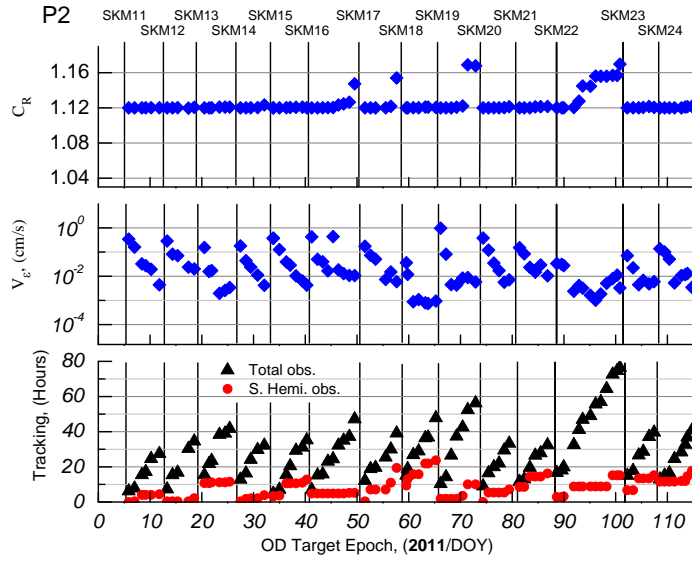


Figure B-7. Overview of P2 SKM sequence for 2011 (through DOY 115) with parameters: $C_R^0 = 1.12$, $\sigma^0 = 0.10$.

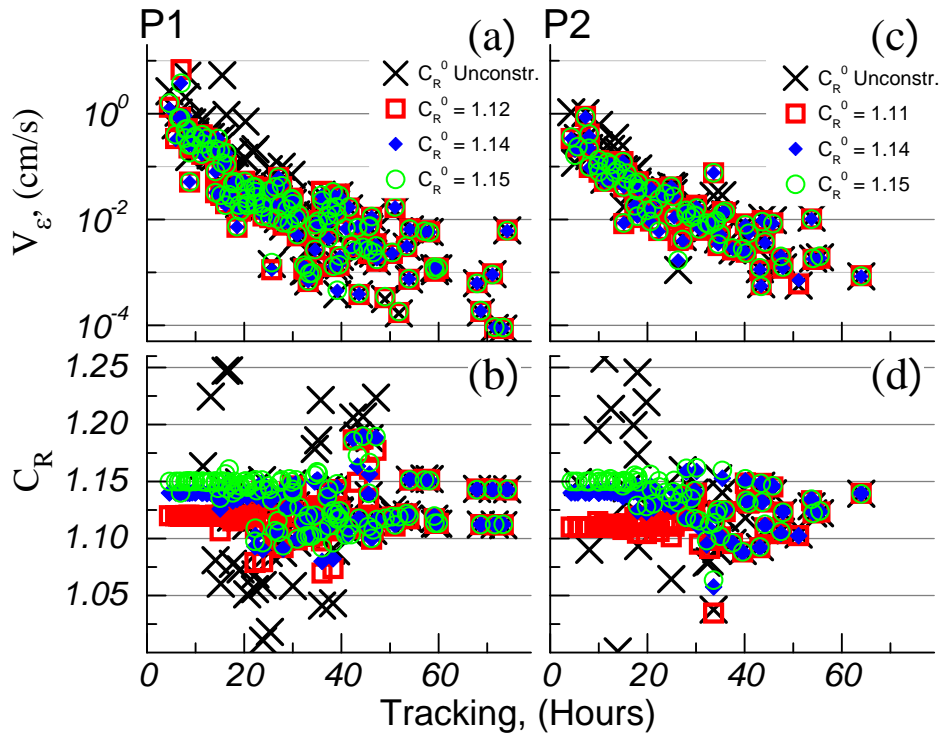


Figure B-8. Comparison of ranges of C_R^0 (along with the unconstrained case) for P1, panels (a) and (b) and P2, panels (c) and (d), across the series of SKMs through DOY 2010/361. The value used for $\sigma^0 = 1.00$, for the constrained data.

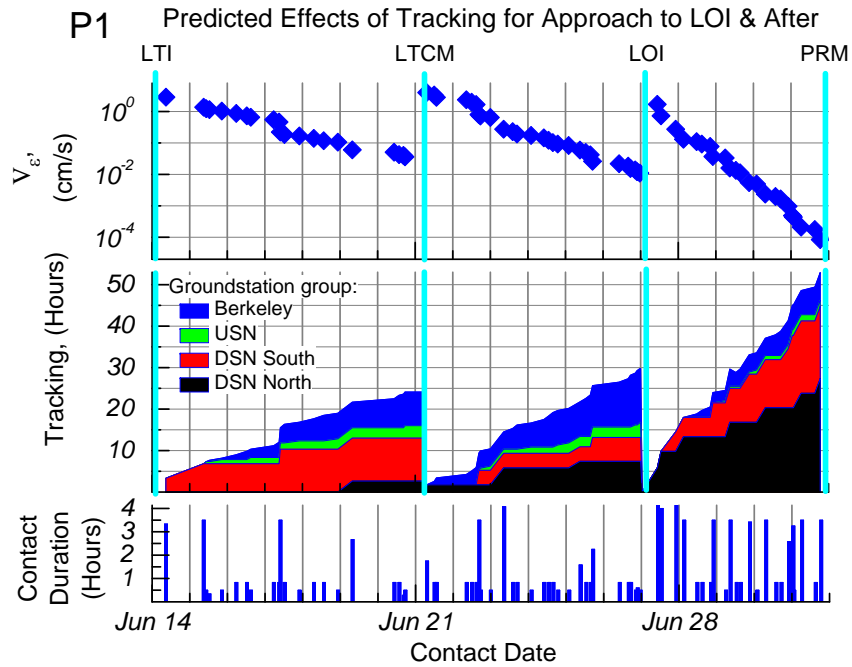


Figure B-9. Predictions of tracking effects on orbit solution uncertainty for P1. This was used for operations planning to ensure enough tracking was scheduled to improve orbit knowledge for the sequence of maneuvers leading up to, including and subsequent to Lunar Orbit Insertion (LOI). LTI refers to the maneuver known as Lunar Transfer Initiation. LTCM was a Lunar Trajectory Control Maneuver. PRM was the first of several Period Reduction Maneuvers.

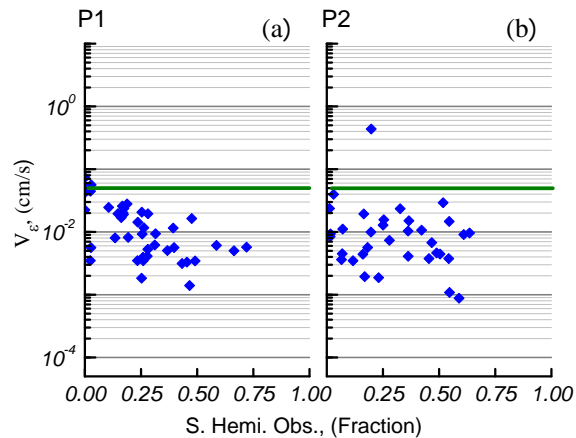


Figure B-10. OD uncertainty as a function of fraction of total data observations from the Southern Hemisphere for aggregated data through DOY 2011/115. Data points represent OD solutions which are based on ~ 25 -30 hours of tracking time. The green horizontal line represents the threshold in OD uncertainty for maneuver planning. Parameters for P1—in panel (a)—were: $C_R^0 = 1.14$, $\sigma^0 = 0.10$; and for P2—in panel (b) were: $C_R^0 = 1.12$, $\sigma^0 = 0.10$.

APPENDIX C: TABLES

Table C-1. Average OD uncertainty and the related standard deviation for P1 $\sigma^0 = 1.00$

C_R^0	$\langle V_\varepsilon^C \rangle$, (cm/s)	$\sigma(V_\varepsilon^C)$
1.12	$2.00 \cdot 10^{-2}$	$1.70 \cdot 10^{-2}$
1.13	$1.97 \cdot 10^{-2}$	$1.61 \cdot 10^{-2}$
1.14	$1.84 \cdot 10^{-2}$	$1.78 \cdot 10^{-2}$
1.15	$1.92 \cdot 10^{-2}$	$1.73 \cdot 10^{-2}$
1.15	$1.95 \cdot 10^{-2}$	$1.74 \cdot 10^{-2}$

Table C-2. Average OD uncertainty and the related standard deviation for P1 $C_R^0 = 1.14$

σ^0	$\langle V_\varepsilon^C \rangle$, (cm/s)	$\sigma(V_\varepsilon^C)$
< 0.10	<i>Poor solver convergence</i>	
0.10	$1.40 \cdot 10^{-2}$	$1.47 \cdot 10^{-2}$
0.20	$1.60 \cdot 10^{-2}$	$1.76 \cdot 10^{-2}$

Note that without constraining C_R^0 , $\langle V_\varepsilon^C \rangle = 3.32 \cdot 10^{-2}$, with $\sigma(V_\varepsilon^C) = 3.00 \cdot 10^{-2}$

Table C-3. Average OD uncertainty and the related standard deviation for P2 $\sigma^0 = 1.00$

C_R^0	$\langle V_\varepsilon^C \rangle$, (cm/s)	$\sigma(V_\varepsilon^C)$
1.11	$1.211 \cdot 10^{-2}$	$1.09 \cdot 10^{-2}$
1.12	$1.205 \cdot 10^{-2}$	$1.05 \cdot 10^{-2}$
1.13	$1.212 \cdot 10^{-2}$	$1.11 \cdot 10^{-2}$
1.14	$1.218 \cdot 10^{-2}$	$1.11 \cdot 10^{-2}$
1.15	$1.239 \cdot 10^{-2}$	$1.12 \cdot 10^{-2}$

Table C-4. Average OD uncertainty and the related standard deviation for P2 $C_R^0 = 1.12$

σ^0	$\langle V_\varepsilon^C \rangle$, (cm/s)	$\sigma(V_\varepsilon^C)$
< 0.10	<i>Poor solver convergence</i>	
0.10	$9.12 \cdot 10^{-3}$	$1.12 \cdot 10^{-2}$
0.20	$9.79 \cdot 10^{-3}$	$1.09 \cdot 10^{-2}$
0.50	$1.22 \cdot 10^{-2}$	$1.07 \cdot 10^{-2}$

Note that without constraining C_R^0 , $\langle V_\varepsilon^C \rangle = 1.61 \cdot 10^{-2}$, with $\sigma(V_\varepsilon^C) = 1.55 \cdot 10^{-2}$

REFERENCES

- [1] D.C. Folta, M.A. Woodard, and D. Cosgrove, "Stationkeeping of the First Earth-Moon Libration Orbiters: The ARTEMIS Miss," *Proceedings of The 2011 AAS/AIAA Astrodynamics Specialist Conference*, Girdwood, AK, July 31-August 4, 2011.
- [2] M. Woodard, D. Cosgrove, P. Morinelli, J.E. Marchese, B.D. Owens, and D. Folta, "Orbit Determination Of Spacecraft In Earth-Moon L1 And L2 Libration Point Orbits," *Proceedings of The 2011 AAS/AIAA Astrodynamics Specialist Conference*, Girdwood, AK, July 31-August 4, 2011.
- [3] T. Pavlak and K. Howell, "Evolution of the Out-of-Plane Amplitude For Quasi-Periodic Trajectories in the Earth-Moon System," *Proceedings of The International Astronautical Congress*, Cape Town, South Africa, October 2011.
- [4] M. Woodard, D. Folta, and D. Woodfork "ARTEMIS: The First Mission to the Lunar Libration Points," *Proceedings of The 2009 International Symposium on Space Flight Dynamics*, Toulouse, France, September 28-October 2, 2009.